

Detection of electrostatic molecular binding using the water proton signal

Yang Zhou^{1,2,3}  | Chongxue Bie^{1,2,4}  | Peter C. M. van Zijl^{1,2} | Jiadi Xu^{1,2}  |
Chao Zou³  | Nirbhay N. Yadav^{1,2} 

¹F.M. Kirby Research Center for Functional Brain Imaging, Kennedy Krieger Institute, Baltimore, MD, USA

²The Russell H. Morgan Department of Radiology, The Johns Hopkins University School of Medicine, Baltimore, MD, USA

³Key Laboratory for Magnetic Resonance and Multimodality Imaging of Guangdong Province, Shenzhen Institute of Advanced Technology, Chinese Academy of Sciences, Shenzhen, Guangdong, China

⁴Department of Information Science and Technology, Northwest University, Xi'an, China

Correspondence

Nirbhay N. Yadav, F.M. Kirby Research Center for Functional Brain Imaging, Kennedy Krieger Institute, 707 N. Broadway, Baltimore, MD 21205, USA; or The Russell H. Morgan Department of Radiology, The Johns Hopkins University School of Medicine, 720 Rutland Ave, Baltimore, MD 21205, USA.
Email: nyadav@jhu.edu

Funding information

China Scholarship Council, Grant/Award Number: 201906970024; Key Laboratory for Magnetic Resonance and Multimodality Imaging of Guangdong Province, Grant/Award Number: 2020B1212060051; National Natural Science Foundation of China, Grant/Award Number: 82171904; National Institutes of Health, Grant/Award Numbers: EB015032, EB025295, EB031771; SIAT Innovation Program for Excellent Young Researchers

Purpose: Saturation transfer MRI has previously been used to probe molecular binding interactions with signal enhancement via the water signal. Here, we detail the relayed nuclear overhauser effect (rNOE) based mechanisms of this signal enhancement, develop a strategy of quantifying molecular binding affinity, i.e., the dissociation constant (K_D), and apply the method to detect electrostatic binding of several charged small biomolecules. Another goal was to estimate the detection limit for transient receptor-substrate binding.

Theory and Methods: The signal enhancement mechanism was quantitatively described by a three-step magnetization transfer model, and numerical simulations were performed to verify this theory. The binding equilibria of arginine, choline, and acetyl-choline to anionic resin were studied as a function of ligand concentration, pH, and salt content. Equilibrium dissociation constants (K_D) were determined by fitting the multiple concentration data.

Results: The numerical simulations indicate that the signal enhancement is sufficient to detect the molecular binding of sub-millimolar ($\sim 100 \mu\text{M}$) concentration ligands to low micromolar levels of molecular targets. The measured rNOE signals from arginine, choline, and acetyl-choline binding experiments show that several magnetization transfer pathways (intra-ligand rNOEs and intermolecular rNOEs) can contribute. The rNOEs that arise from molecular ionic binding were influenced by pH and salt concentration. The molecular binding strengths in terms of K_D ranged from 70–160 mM for the three cations studied.

Conclusion: The capability to use MRI to detect the transient binding of small substrates paves a pathway towards the detection of micromolar level receptor-substrate binding in vivo.

KEYWORDS

acetyl-choline, arginine, choline, dissociation constant, electrostatic interaction, exchange relayed NOE, IMMOBILISE, molecular binding, saturation transfer MRI

Yang Zhou and Chongxue Bie contributed equally to this work.

This is an open access article under the terms of the Creative Commons Attribution-NonCommercial-NoDerivs License, which permits use and distribution in any medium, provided the original work is properly cited, the use is non-commercial and no modifications or adaptations are made.

© 2022 The Authors. *Magnetic Resonance in Medicine* published by Wiley Periodicals LLC on behalf of International Society for Magnetic Resonance in Medicine.

1 | INTRODUCTION

Electrostatic interactions play a fundamental role in mediating molecular interactions and are essential in many biochemical processes.¹ One of the most common methods for probing intra- and intermolecular interactions in NMR spectroscopy is via nuclear Overhauser effects (NOEs).^{2,3} When two protons are in close proximity, a magnetic perturbation of one proton can be transferred to the other via dipolar cross-relaxation, leading to NOEs. The magnitude of NOEs decreases very rapidly with increasing interproton distance, thus nuclear overhauser effect (NOE)-based NMR methods^{3,4} are widely used to study molecular interactions between molecules in close proximity. While the use of NMR spectroscopy to characterize intermolecular interactions is common,^{3,5} imaging studies have been limited due to the sensitivity and concomitant low spatial resolution when studying millimolar concentration molecules.

Saturation transfer (ST) or chemical exchange saturation transfer (CEST) MRI methods have demonstrated a promising approach for enhancing the signal from low concentration solute molecules using the water proton signal.^{6–9} ST approaches can report on magnetic coupling between solute molecules and water which can occur directly (e.g., chemical exchange¹⁰) or involve several magnetization transfer pathways (e.g., NOE^{11–13} or J-coupling^{14,15}). Recently, it was shown that transient molecular binding could be imaged using a saturation transfer approach for enhancing sensitivity.¹⁶ This so-called IMMOBILISE (for “IMaging of MOlecular BInding using Ligand Immobilization and Saturation Exchange”) technique relies on the phenomenon that, upon binding to immobile receptors, magnetically labeled non-exchangeable protons in ligands can couple efficiently to water via relayed NOEs (rNOEs), i.e., fast cross-relaxation (spin diffusion) over the solid proton pools relayed to water via chemical exchange of either protons or water molecules. This approach thus exploits ST from protons on the bound ligand via protons on the immobile or less mobile¹³ macromolecular complex to the water. While the first step is similar to ST methods used commonly in high-resolution NMR,^{3,5} the major strength of the method lies in the second step of transfer to water protons, allowing actual imaging of the binding of millimolar (mM) levels of natural (no chemical labeling) ligands.

Here, the binding of small charged molecules (L-arginine, choline, and acetyl-choline) via electrostatic interactions to immobile ionic receptors was systematically studied using water saturation spectroscopy (Z-spectroscopy¹⁷). The mechanism of water signal

enhancement through molecular binding was also elucidated. Depending on the molecular composition in terms of proton pools, both intramolecular (within the binding complex) and intra-ligand rNOEs can play a role. We derived a model to analytically describe this process and utilized it to quantitatively evaluate binding affinities for the above molecules based on the changes in water signal.

2 | METHODS

2.1 | Theory

The IMMOBILISE experiment¹⁶ resembles a routine CEST experiment in that it consists of a period of selective radiofrequency (RF) based magnetic labeling of protons on low-concentration molecules, followed by observing the buildup of a signal reduction (saturation) of the bulk water signal. The latter is due to repeated label transfers, which allow detection of the presence of these solute molecules with enhanced sensitivity using the water signal in MRI. However, unlike a CEST experiment which targets exchangeable protons (e.g., $-OH$, $-NH$, $-NH_2$) exchanging directly with water, an IMMOBILISE experiment labels the aliphatic protons ($-CH_n$) of free ligands. Normally this label would not be transferrable to the water signal with sufficient intensity, but if ligand binds to another molecule (receptor) with a possible magnetization transfer pathway to water, this becomes possible. Repeated binding followed by multiple label transfers then again causes a signal enhancement effect that can be imaged. Figure 1 shows three possible binding-mediated saturation transfer pathways from a ligand proton to water, all of which are initiated by a ligand binding to an immobile receptor, followed by an intramolecular proton–proton NOE transfer within the binding complex and a final transfer of label to the water. Within the small fast-tumbling ligands, intramolecular NOE transfer is very weak. However, upon binding to immobile receptors, the cross-relaxation becomes very efficient (spin diffusion) thus allowing the labeled ligands to couple to water via multiple rNOEs (Figure 1). The saturation transfer pathways in general can be categorized into two scenarios. (i) Intermolecular NOE: the magnetic label on the ligand is transferred to the resin upon binding via spin diffusion, and then to free water either via chemical exchange of resin protons or via water exchange (Figures 1A, B); (ii) Intramolecular NOE: upon binding, the magnetic label on the aliphatic protons of the ligand is rapidly transferred via spin diffusion to exchangeable protons within the molecule, and then to water via chemical exchange (Figure 1C).

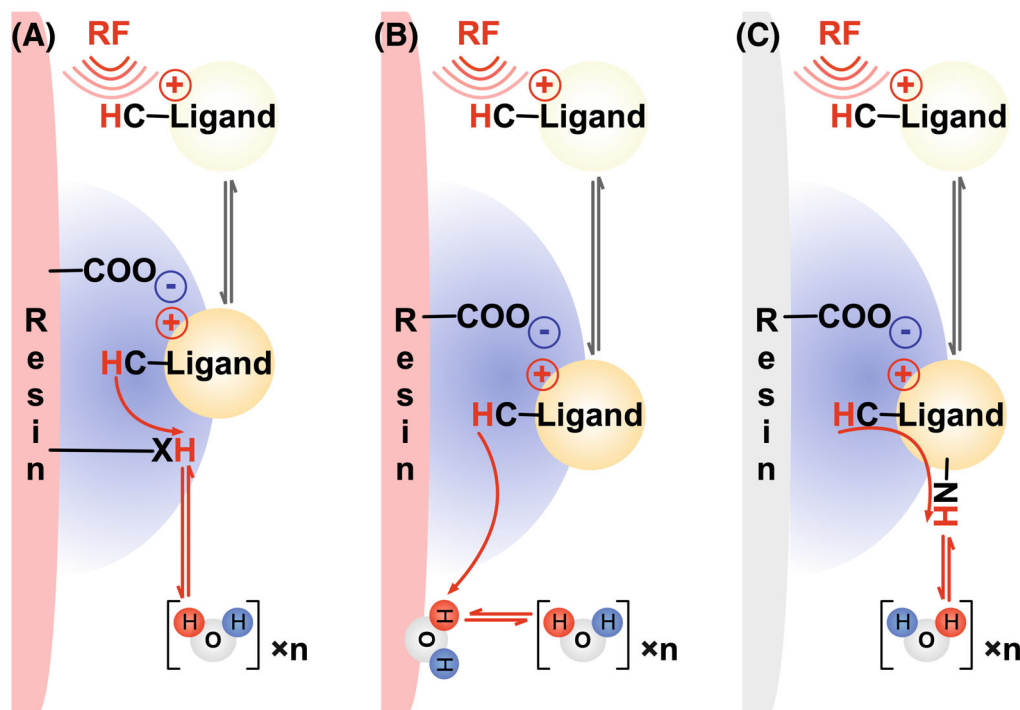
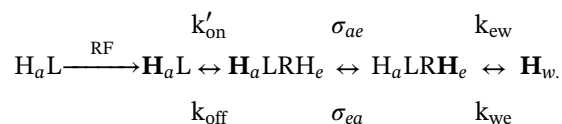


FIGURE 1 Possible pathways of NOE-based saturation transfer during electrostatic binding of a small molecule to an immobile resin. The aliphatic protons of free ligand are efficiently labeled by an RF pulse, and there is negligible NOE based transfer within the fast tumbling molecule. Upon binding, the tumbling rate of the ligand is greatly reduced and fast spin-diffusion-based saturation transfer pathways from ligand aliphatic protons to free water protons are feasible: *intermolecular NOE* – the labeled magnetization is transferred (indicated in red) through space via spin diffusion processes to (A) an exchangeable proton on the immobile resin or (B) water bound to the resin, and then to free water via either proton chemical exchange ($-XH$) or water molecular exchange, respectively. The third pathway is via *intramolecular NOE*, where the labeled magnetization on aliphatic protons is transferred to exchangeable protons within molecule via spin diffusion (C), and then to free water via proton chemical exchange

Since all of the three possible ST pathways in Figure 1 begin with the reversible binding of RF labeled (or saturated) free ligands and end with the labeling reaching bulk free water, this general ST process from free ligands to water was described by the same three-step model (see below). We are using the terminology saturation transfer here, but in principle, the mechanism is general for all labeling of magnetization, e.g., inverted magnetization or any other perturbation in the magnetization ultimately leading to water signal change. Initially, aliphatic protons (H_a) are labeled (labeled protons denoted in boldface: \mathbf{H}_a) using RF irradiation while on free ligand (L). There is negligible saturation transfer from these non-exchangeable free ligand protons to water. The ligand then binds transiently to the immobile resin macromolecule (\mathbf{H}_aLR), during which magnetization (saturation) is transferred via spin diffusion to either (i) exchangeable protons in the macromolecular complex or to (ii) bound water molecules/protons in the macromolecular complex (both indicated by LRH_e). Notice that this model includes exchangeable protons or bound water in either the bound ligand or the resin as they are part of an immobile complex (LR). Finally, magnetization is

transferred to free water protons (H_w) either through proton exchange or water exchange, which is why we use the nomenclature of relayed NOE (rNOE) for these two possible pathways:



where k_{on} and k_{off} are ligand binding on/off rates. At the binding equilibrium, $k_{on}[R][L] = k_{off}[LR]$, where $[L]$, $[R]$ and $[LR]$ are the concentrations of free ligands, free receptor, and bound receptor, respectively. Total receptor concentration $[R_T] = [LR] + [R]$. Notice that k_{off} is a first order rate constant with units of s^{-1} , while k_{on} is a second order rate constant with units $M^{-1} s^{-1}$. For the unit equivalence, we use $k'_{on} = k_{on}[R]$ in the equations. σ_{ae} and σ_{ea} the effective cross relaxation rates from receptor-bound-ligand aliphatic protons (H_aLR) to either exchangeable protons (LRH_e) or bound water in the macromolecule and back. Finally, k_{ew} and k_{we} are effective saturation transfer rates from exchangeable protons in the immobile complex

(LRH_e) to free water (H_w) and back, corresponding to either the proton or water molecular exchange rates. Notice the similarity to a previous model describing rNOE transfer in glycogen,¹³ which is now preceded by a ligand binding step. A main difference is that the cross-relaxation transfer step in the solid (tens of thousands in s^{-1}) is much faster than in glycogen (order of tens in s^{-1}) and depending on the exchange rate k_{ew} and the speed of binding and dissociation, this ligand binding step may become superfluous in the model.

In saturation transfer experiments, a continuous saturation pulse is applied on the free ligand aliphatic proton pool (L) resulting in a saturated aliphatic proton pool H_a . The evolution of the z -magnetization for each pool (A = Aliphatic, E = Exchangeable, W = Water) can be described by a set of modified Bloch equations,

$$\frac{dA_z^L}{dt} = -\rho_a^L (A_z^L - A_{z,0}^L) - k'_{on}A_z^L + k_{off}A_z^{LR} - \omega_1 A_y^L \quad (1)$$

$$\begin{aligned} \frac{dA_z^{LR}}{dt} = & -\rho_a^{LR} (A_z^{LR} - A_{z,0}^{LR}) - \sigma_{ea} (E_z^{LR} - E_{z,0}^{LR}) \\ & + k'_{on}A_z^L - k_{off}A_z^{LR} \end{aligned} \quad (2)$$

$$\begin{aligned} \frac{dE_z^{LR}}{dt} = & -\rho_e^{LR} (E_z^{LR} - E_{z,0}^{LR}) - \sigma_{ae} (A_z^{LR} - A_{z,0}^{LR}) \\ & - k_{ew} E_z^{LR} + k_{we} W_z \end{aligned} \quad (3)$$

$$\frac{dW_z}{dt} = -\rho_w (W_z - W_{z,0}) + k_{ew} E_z^{LR} - k_{we} W_z \quad (4)$$

ρ_a^L , ρ_a^{LR} , ρ_e^{LR} , ρ_w are the longitudinal auto-relaxation rates for the aliphatic proton of free ligand (L , or H_aL), aliphatic proton of bound ligand (H_aLRH_e), exchangeable proton or bound water of immobile complex (H_aLRH_e), and free water proton (H_w) pools. ω_1 is the radial frequency corresponding to the B_1 field. Importantly, the auto-relaxation rate ρ_a^L has contributions from T_1 relaxation and cross-relaxation, i.e., $\rho_a^L = 1/T_{1a}^L - \sigma_{ae}$, while $\rho_a^L = 1/T_{1a}^L$ in the small molecules ($-\sigma_{ae} \approx 0$), the auto-relaxation rates in the bound complex are given by $\rho_a^{LR} = 1/T_{1a}^{LR} - \sigma_{ae} \approx -\sigma_{ae}$ ($-\sigma_{ae} \gg 1/T_{1a}^{LR}$). Notice that here T_{1a}^L is the relaxation time for free ligand, which can be measured in solution without resin. Since ρ_a^{LR} and σ_{ae} are of the same order of magnitude but opposite sign, the magnitude of T_{1a}^{LR} is still reasonably long (100 ms or more), allowing us to perform NMR experiments. When the ligand is bound, the signals broaden and cannot be efficiently saturated, so no ω_1 term is included. Assuming steady-state is reached, and $\frac{dA_z^L}{dt} = 0$, $\frac{dA_z^{LR}}{dt} = 0$, $\frac{dE_z^{LR}}{dt} = 0$, $k_{ew}E_{z,0} - k_{we}W_{z,0} = 0$, and $k'_{on}A_{z,0}^L - k_{off}A_{z,0}^{LR} = 0$. We can then obtain the analytical

solution for the percentage of water labeling, i.e., rNOE signal (see details in Supporting Information):

$$\text{rNOE} \equiv \frac{W_{z,0} - W_z}{W_{z,0}} = \alpha \cdot \beta \cdot f \quad (5)$$

where α is the saturation efficiency of B_1 on ligand aliphatic protons, $\alpha = \frac{(A_{z,0}^L - A_z^L)}{A_{z,0}^L}$; $\alpha = 1$ when the ligand proton pool is fully saturated (i.e., $A_z^L = 0$). The exact analytical solution of α is difficult to derive due to the system complexity, yet can be approximated by treating L as a single proton pool under an on-resonance B_1 field:

$$\alpha \approx \frac{T_{1a}^{L'} T_{2a}^{L'} \omega_1^2}{1 + T_{1a}^{L'} T_{2a}^{L'} \omega_1^2} \quad (6)$$

where $T_{1a}^{L'}$ and $T_{2a}^{L'}$ are the “effective” relaxation times for ligands, which in principle could be measured when ligands are mixed with resin (note its difference with T_{1a}^L).¹⁸ $f = \frac{A_{z,0}^L}{W_{z,0}} = \frac{n_a[L]}{2[H_2O]}$, is the ratio of the equilibrium magnetizations of the saturated aliphatic protons and the water protons, with n_a the number of protons in the aliphatic pool and 2 the number of water protons. $[H_2O]$ is the water concentration. β is the enhancement factor,

$$\beta = \frac{k_{ew}\sigma_{ae}k'_{on}}{\left(\begin{aligned} & \sigma_{ea}\sigma_{ae}\rho_w + \sigma_{ea}\sigma_{ae}k_{we} - k_{off}\rho_e^{LR}\rho_w - k_{off}k_{ew}\rho_w \\ & - k_{off}\rho_e^{LR}k_{we} - \rho_a^{LR}\rho_e^{LR}\rho_w - \rho_a^{LR}k_{ew}\rho_w - \rho_a^{LR}\rho_e^{LR}k_{we} \end{aligned} \right)} \quad (7)$$

In the slow tumbling limit, we assume $-\sigma_{ea} \approx -\sigma_{ae} \approx \rho_a^{LR} \approx \rho_e^{LR} \gg \rho_w$, and β can be rewritten as,

$$\begin{aligned} \beta & \approx \frac{-k_{ew}\sigma_{ae}k'_{on}}{k_{off}\rho_e^{LR}\rho_w + k_{off}k_{ew}\rho_w + k_{off}\rho_e^{LR}k_{we} + \rho_a^{LR}k_{ew}\rho_w} \\ & \approx \frac{1}{\left(\frac{\rho_w}{k_{ew}} + \frac{k_{we}}{k_{ew}} + \frac{\rho_w}{-\sigma_{ae}} + \frac{\rho_w}{k_{off}} \right)} \frac{k'_{on}}{k_{off}} \end{aligned} \quad (8)$$

and

$$\begin{aligned} \text{rNOE} & \approx \alpha \cdot \frac{1}{\left(\frac{\rho_w}{k_{ew}} + \frac{k_{we}}{k_{ew}} + \frac{\rho_w}{-\sigma_{ae}} + \frac{\rho_w}{k_{off}} \right)} \cdot \frac{n_a[L]k'_{on}}{2[H_2O]k_{off}} \\ & = \alpha \cdot \beta' \cdot \frac{n_a[LR]}{2[H_2O]} \end{aligned} \quad (9)$$

It is useful to rewrite $[LR]$ using known parameters: $[R_T]$, total receptor concentration, $[L]$, free ligand concentration, f_R , the fraction of receptor in bound state, and K_D

($K_D = \frac{k_{off}}{k_{on}}$), the dissociation constant^{4,19,20}:

$$[LR] = [R_T] \cdot f_R = [R_T] \cdot \frac{[L]}{[L] + K_D} \quad (10)$$

From Equations (9) and (10), it can be seen that the detected rNOE signal in the binding system is linearly dependent on the population of ligand in the bound state ($[LR]$), which is a function of free ligand concentration ($[L]$) and the strength of the electrostatic interaction or the binding equilibrium.^{4,19} Then the rNOE signal can be rewritten as:

$$\text{rNOE} = \alpha \cdot \beta' \cdot \frac{n_a [R_T]}{2[\text{H}_2\text{O}]} \cdot \frac{[L]}{[L] + K_D} = \text{rNOE}_{\text{max}} \cdot \frac{[L]}{[L] + K_D} \quad (11)$$

where $\text{rNOE}_{\text{max}} = \alpha \cdot \beta' \cdot \frac{n_a [R_T]}{2[\text{H}_2\text{O}]}$, is a constant that determines the maximum detected signal.

Two extreme cases can be distinguished: first, when binding is extremely weak, $k_{off} \rightarrow \infty$ (or $K_D \rightarrow \infty$), the rNOE signal will be zero (as $\frac{[L]}{[L] + K_D} \rightarrow 0$). Second, when binding is extremely strong, $k_{off} \rightarrow 0$ ($\frac{\rho_w}{k_{off}} \rightarrow \infty$), then,

$$\beta' = \frac{1}{\left(\frac{\rho_w}{k_{ew}} + \frac{k_{we}}{k_{ew}} + \frac{\rho_w}{-\sigma_{ae}} + \frac{\rho_w}{k_{off}} \right)} \approx \frac{1}{\left(\frac{\rho_w}{k_{off}} \right)} = k_{off} \cdot T_{1W} \rightarrow 0 \quad (12)$$

The equations suggest that the rNOE signal will not be generated for extremely strong or weak binding processes and applicable only for reversible binding equilibria, as also supported by simulation data (Figure 2).

2.2 | Sample preparation

Sample pH may affect saturation transfer efficiency when exchangeable protons are involved, while salt concentration is expected to affect electrostatic binding.²¹ To study ST and binding effects of small positively charged ligands to a negatively charged ion-exchange resin, the following samples were prepared:

L-arginine (Arg, from Sigma Aldrich, St Louis, MO) solutions in phosphate-buffered saline (PBS): (A) 100 mM ligand, pH values of 6.0, 6.5, 7.0, 7.2, 7.5, 8.0, 9.0, 10.0, 11.0, and 12.0 without adding salt; (B) 100 mM ligand, salt concentrations of 0, 25, 50, 100, 200, 500 and 1000 mM at pH of 7.2. (C) Ligand concentrations of 10, 20, 50, 100, and 200 mM at pH of 7.2, without adding salt.

Acetyl-choline (ACh) and choline (Cho) solutions in PBS, using Acetyl-choline Chloride and Choline Chloride, respectively (Sigma Aldrich, St Louis, MO): (D) 50 mM ligand, pH values of 4.0, 5.0, 5.5, 6.0, 6.5, 7.2, 8.0, 8.5, 9.0, and 10.0 without adding salt; (E) 50 mM ligand, salt

concentrations of 0, 100, 200, 500, 1000 and 2000 mM at pH of 7.2. (F) Ligand concentrations of 10, 20, 50, 100, and 200 mM at pH of 7.2, without adding salt.

The ion-exchange resin (Macro-Prep CM Support, with functional groups $-\text{COO}^-$, from Bio-Rad Laboratories, Inc., Hercules, CA) was washed first with 4M NaCl (5 times with 10 mL each time) and then with PBS (10 times, 10 mL each time) before use. Each of the solutions (A–F) was used first to wash the ion-exchange resin (4 times with 4 mL each time) and then an additional 4 mL was mixed with ion-exchange resin. The pH of the mixtures was checked again. Then mixture (including ~ 0.5 mL ion-exchange resin and 0.5 mL solution) was transferred to the imaging tube for ST measurements.

2.3 | CEST MRI

Experiments were performed on a Bruker Avance III 17.6 T vertical bore MR scanner (Bruker Biospin, Ettlingen, Germany) with a 20 mm SAW-type micro-imaging transmit/receive coil at 20 °C, using a 4 s continuous-wave radiofrequency (RF) saturation pulse followed by a rapid acquisition with relaxation enhancement MRI readout. A 5 mm slice within sediment in the tube was chosen for ST MRI measurements. Z-spectra were acquired by stepping the irradiation frequency over the proton spectral range (± 6 ppm relative to water in steps of 0.1 ppm), and displayed by normalizing the saturated water signal intensity (S) with the signal intensity without saturation (S_0 , acquired at $B_1 = 0$ μT). The B_1 strength was varied from 0.3 to 2.0 μT . Z-spectral shifts caused by B_0 inhomogeneities between tubes and voxels within tubes were corrected using the WASSR method.²² To eliminate the mismatch of the background signal when comparing Z-spectra between tubes, Z-spectral intensities (S/S_0) were further referenced to the Z-spectral intensity at 6 ppm of ion-exchange resin.²³ Z-spectral components were analyzed using multi-Lorentzian fitting, as described previously.¹³ And the rNOE signals were quantified by peak intensity of Lorentzian lineshape.

3 | RESULTS

3.1 | Numerical simulations

Using the four-pool Bloch equation modeling, numerical simulations were conducted to gain further insights into the quantitative relation between binding and rNOE signal (parameters used in the simulations are in Table 1, simulation protocols are in Supporting Information). Figures 2A, B show the CEST Z-spectra for binding

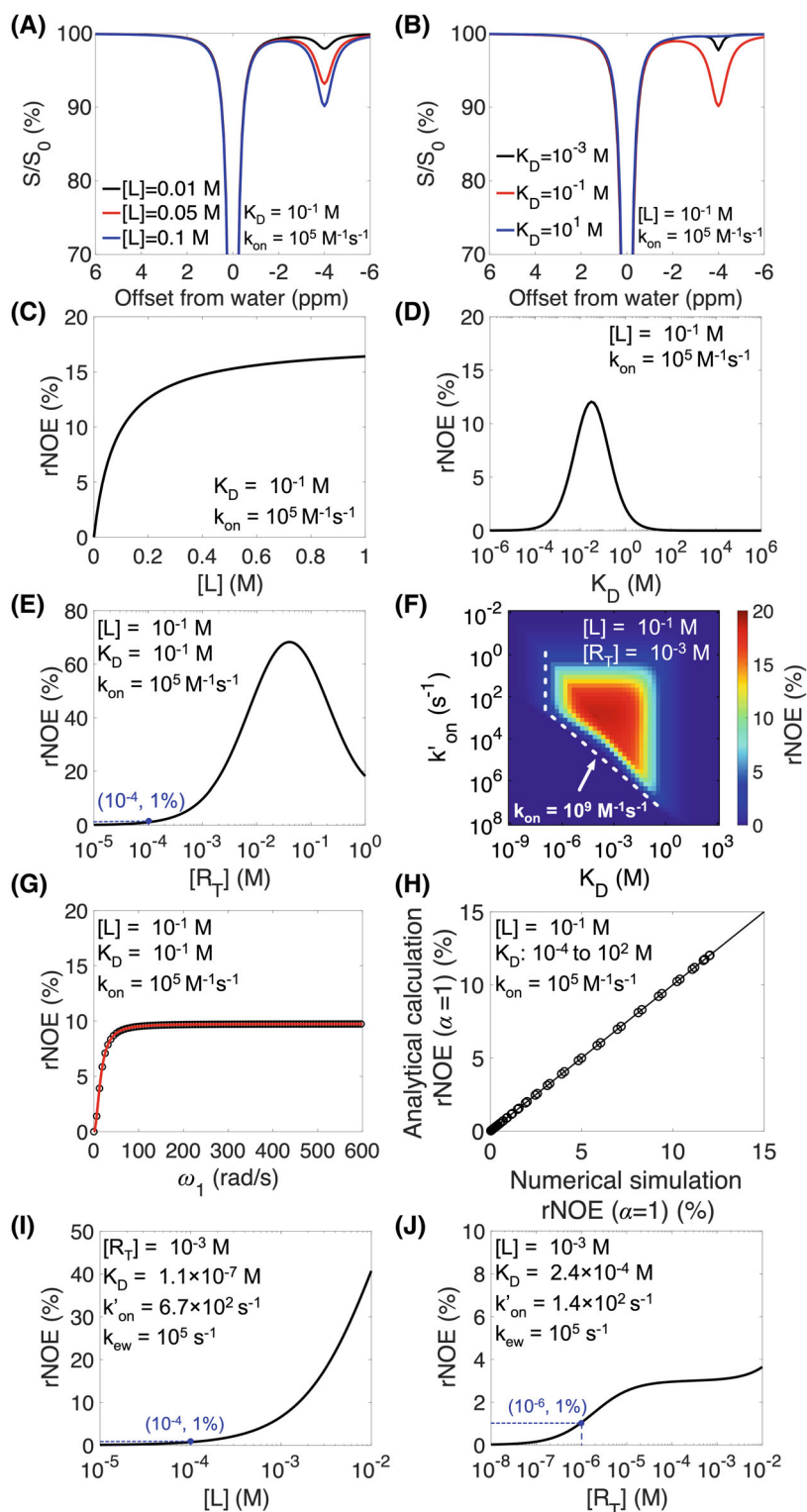


FIGURE 2 Numerical simulations of rNOE signal in ST MRI of ligand binding. The simulated rNOE signal dependence on (A, C) concentration of free ligand ($[L]$), (B, D) binding affinity (K_D), (E) total receptor concentration ($[R_T]$), and (F) K_D and binding rates (k_{on}). The upper limit of k_{on} was set to be $10^9 \text{ M}^{-1} \text{ s}^{-1}$.⁴ $\omega_1 = 600 \text{ rad/s}$. (G) The dependence of simulated rNOE signal (black circles) intensities on the radial frequency based on B_1 field strength is in agreement with that using the analytical solution (red line, using Equation 6). (H) The rNOE signals ($\alpha = 1$) from numerical simulation using the Bloch equations are in agreement with those from analytical calculation. (I, J) Estimation of the lower limits for ligand and receptor concentrations using optimized conditions for the binding rate and exchange transfer rate. Simulation parameters are in Table 1, unless specified, k_{ew} was 10^3 s^{-1}

equilibria with varied free ligand concentration ($[L]$) and binding affinity (K_D), respectively. Compared to a ^1H NMR spectrum, the Z-spectrum shows the relative amount of water saturation (S/S_0 , with S_0 the non-saturated signal) when irradiating at a certain frequency in the proton NMR spectrum. Because the Z-spectrum reports only on the water signal, Z-spectra are referenced to the water

signal at 4.7 ppm, now assigned to 0 ppm. Simulated rNOE signal (resonance set at -4 ppm referenced to water, Figures 2A, B) increases with $[L]$ and reaches a plateau as receptors get saturated with increasing $[L]$ (Figure 2C), in good agreement with Equation (11). The rNOE signal first increases and then decreases with an increase in K_D (Figures 2B, D). The suitable ranges of total receptor

TABLE 1 Values of the parameters as set in numerical simulations

Parameters	Values	Parameters	Values	Parameters	Values
ρ_a^L (s ⁻¹)	0.56 ^a	λ_a^L (s ⁻¹)	1.67 ^a	Ω_a^L (ppm)	-4 or -20
ρ_a^{LR} (s ⁻¹)	$-\sigma_{ea}$	λ_a^{LR} (s ⁻¹)	$-2.5 \times \sigma_{ea}^c$	Ω_a^{LR} (ppm)	-4 or -20
ρ_e^{LR} (s ⁻¹)	$-\sigma_{ea}$	λ_e^{LR} (s ⁻¹)	$-2.5 \times \sigma_{ea}^c$	Ω_e^{LR} (ppm)	1.2 ^e
ρ_w (s ⁻¹)	0.36 ^a	λ_w (s ⁻¹)	0.56 ^a	Ω_w (ppm)	0
[L] (M)	10 ⁻⁵ to 1 ^b	σ_{ea}, σ_{ae} (s ⁻¹)	-5×10^{5d}	K_D (M)	10 ⁻⁹ to 10 ^{3b}
[LR _a] (M)	$n_a[LR]$	k_{ew} (s ⁻¹)	1000 ^e	k'_{on} (s ⁻¹)	10 ⁻² to 10 ^{8b}
[LR _e] (M)	[LR _a]	k_{we} (s ⁻¹)	$k_{ew} \cdot \frac{[LR_e]}{2[H_2O]}$	k_{off} (s ⁻¹)	$K_D \cdot k_{on}$
[H _w] (M)	2[H ₂ O]	μ_{ae} (s ⁻¹)	$-2 \times \sigma_{ea}^c$	[R _T] (M)	10 ^{-3f}

L : free ligand R: receptor; LR: receptor-bound-ligand; a : aliphatic protons; e : exchangeable protons or bound water protons in the immobile complex; w: water; H_w: free water protons; [...]: concentration; ρ: longitudinal auto-relaxation rate (without chemical exchange or dipolar coupling contributions); λ is the transverse auto-relaxation rate (without chemical exchange or dipolar coupling contributions); σ is the effective longitudinal cross-relaxation rate, we assume $\sigma_{ea} = \sigma_{ae}$; μ is the transverse cross-relaxation rate, we assume $\mu_{ae}^{LR} = \mu_{ea}^{LR}$; k_{ew} and k_{we} are the effective exchange rates from LRH_e to water protons and back, respectively; Ω is the chemical shift offset relative to free water protons; K_D, dissociation constant; k'_{on} and k_{off} , ligand binding on and off rates; [LR] is receptor-bound-ligand concentration, here calculated from K_D; n_a is the number of protons in the aliphatic pool (set to 9 in the simulation); [R_T]: total receptor concentration; $k_{on} = 10^5 \text{ M}^{-1} \text{ s}^{-1}$; B₀ field is 17.6 T. Mixing time is 50 s. ω₁ is the angular frequency corresponding to the B₁ field strength, equals to 600 rad/s (2.24 μT).

^aRef.43.

^bAssumed range for fitting.

^cRef.44.

^dRef.17.

^eAssumed based on Ref. 13.

^fEstimated value.

site concentrations ([R_T]), K_D values and binding rates (k'_{on}) for rNOE signal to be detected were simulated and the results are shown in Figures 2E, F. It was found that rNOE is detectable (using 1% of water signal as the rNOE detection threshold) for binding events with slow binding exchange rates (k'_{on} , within about 10¹ to 10⁶ s⁻¹), medium affinity (K_D, within about 10⁻⁷ to 1 M), and above sub-millimolar level of receptor sites ([R_T], larger than about 10⁻⁴ M). From Figure 2G, the dependence of simulated rNOE signal on B₁ field strength shows that the saturation efficiency α and rNOE signal can be described analytically by Equations (6) and (11). The analytical solution for rNOE (Equation 11) is also verified by numerical simulations (Figure 2H). Figures 2I and 2J plot the rNOE signals dependence on [L] and [R_T] with optimum binding and exchange transfer rates. The detection limits for this approach under these conditions are indicated on these plots.

3.2 | Experiments

To test the feasibility of evaluating molecular binding, ST experiments were carried out to study the interaction of several positively charged small molecules with a negatively charged ion-exchange resin (-COO⁻ functional group) used routinely in ion-exchange chromatography.²⁴

Figure 3 shows the results for L-arginine (Arg, positively charged at neutral pH) solution equilibrated with the resin. On the negative side of the Z-spectrum (Figures 3D, S1), three peaks are present at -0.9, -1.6 and -3.0 ppm (notice the overlapping peaks at -2.9 and -3.1 ppm), showing the rNOE-based magnetization transfer from Arg aliphatic protons²⁵ (Figures 3A, B) to water. This is in contrast to the Z-spectrum of Arg solution alone (Figure 3C) which shows only two peaks centered at +1.9 ppm and +2.5 ppm, corresponding to the CEST signals from the guanidinium protons (position a, Figure 3A) and amide protons (position b) of Arg.²⁶ This appearance of rNOE signals in the Z-spectrum of Arg mixed with resin suggests these to be a consequence of the electrostatic-interaction-mediated molecular binding of Arg to immobile carboxyl groups. Notice that these signals originate from the irradiation of free ligand, as the linewidth of protons of bound ligand is too large to show a distinguishable resonance.

To further confirm that the detected Arg rNOE signals arise from the temporary immobilization due to molecular ionic binding, we evaluated the effects of pH and salt concentration (or ionic strength) on the quantified signal, as pH and salt concentration can change the binding strength of ions and therefore the ionic binding equilibrium.²⁷ The signals were quantified as the peak intensities of a Lorentzian lineshape fitted from residual Z-spectra after removing the baseline. Both CEST and rNOE signals

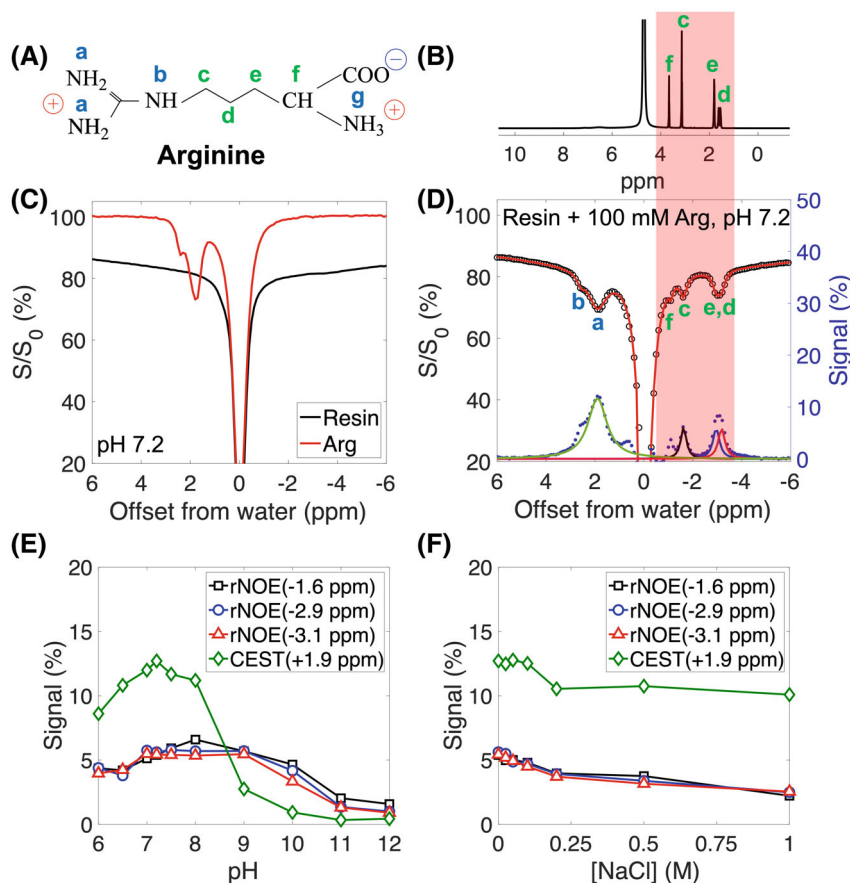


FIGURE 3 Z-spectroscopy of Arg solutions mixed with ionic resin. (A) Chemical structure of Arg. (B) ^1H NMR spectrum of Arg (5% $\text{H}_2\text{O}/95\%$ D_2O , pH 7.2), peak assignments are based on previous studies.^{25,26} (C) Individual Z-spectra ($B_1 = 0.7 \mu\text{T}$, 4 s) of ionic resin and Arg solution (100 mM, pH of 7.2). (D) Experimental (black circle) and fitted (red solid line) Z-spectra of resin with Arg (100 mM, pH of 7.2, $[\text{NaCl}] = 0 \text{ mM}$) using $B_1 = 0.7 \mu\text{T}$, 4 s (left vertical axis). The broad background is caused by the magnetization transfer contrast of the immobile resin to water. The extracted CEST (+1.9 ppm) and rNOE signals (-1.6, -2.9, and -3.1 ppm) are also shown with an intensity scale on the right vertical axis. (E, F) The dependence of fitted CEST and rNOE signal on pH and salt concentration. The rNOE (-2.9 ppm) and rNOE (-3.1 ppm) were fitted with same Lorentzian lineshape but with different chemical shifts

were found to be strongly influenced by pH. The CEST peaks (a and b in Figure 3D) gradually increased from pH 6 to 8,²⁸ but became invisible at high pH (Figures 3E, S2). The rNOE peak intensities at three positions (-1.6, -2.9, and -3.1 ppm, Figure 3E) were about the same and slowly increased in intensity from pH 6 to 8 (similar to the CEST peaks), before dropping at higher pH (but signal still detectable). In addition, the rNOE signal decreased by as much as about 50% as salt concentration increased, while the CEST signal only slightly decreased (Figure 3F).

To evaluate the contributions of possible ST mechanisms (see Figure 1) to the water signal, choline (Cho) and acetyl-choline (ACh) were studied. Both molecules have the same positively charged head group (Figures 4A, D), but ACh has no exchangeable protons and thus no ST pathway to water via intramolecular rNOEs (Figure 2C). The Z-spectra show detection of Cho aliphatic protons at -1.6 ppm (Figures 4C, S3, S4) and ACh aliphatic protons at -1.6 and -2.6 ppm (Figures 4F, S5, S6). Interestingly, the observed ACh rNOE signal was stronger than that of Cho (Figures 4C, F, S7B). Similar to Arg, the rNOE signals from Cho and ACh were found to be small at acidic pH and reach a maximum in the physiological pH range (Figure 4G), and the signals decreased with solvent salt concentration (Figure 4H).

To determine molecular binding affinities, the rNOE signals were measured as a function of free ligand concentration (pH 7.2) and the curves were fitted (Figures 5, S8) using Equation (11) to estimate K_D and rNOE_{max} . The results (Table 2) show that the K_D values fitted from three individual peaks of Arg were the same within error (averaging at about 130 mM). The rNOE_{max} for Arg increased with B_1 strength, as expected from Equation (6). The term $\beta' \cdot \frac{[R_T]}{2[\text{H}_2\text{O}]}$ in rNOE_{max} , indicative of signal enhancement magnitude, was estimated from the rNOE_{max} peak intensity dependence of B_1 , so only one value is retrieved. The Cho and ACh data (Table 3) show that ACh has a higher binding affinity (smaller K_D) with the resin ($-\text{COO}^-$) than Cho at a pH of 7.2 and $[\text{NaCl}] = 0$. The values of $\beta' \cdot \frac{[R_T]}{2[\text{H}_2\text{O}]}$ for Cho and ACh were similar, yet about only half of that for Arg.

4 | DISCUSSION

We demonstrated the use of ST MRI to characterize the ionic binding of small molecules to immobile receptors. The method relies on binding-facilitated saturation transfer from ligand aliphatic protons to other protons in the immobile resin-ligand complex (via inter-

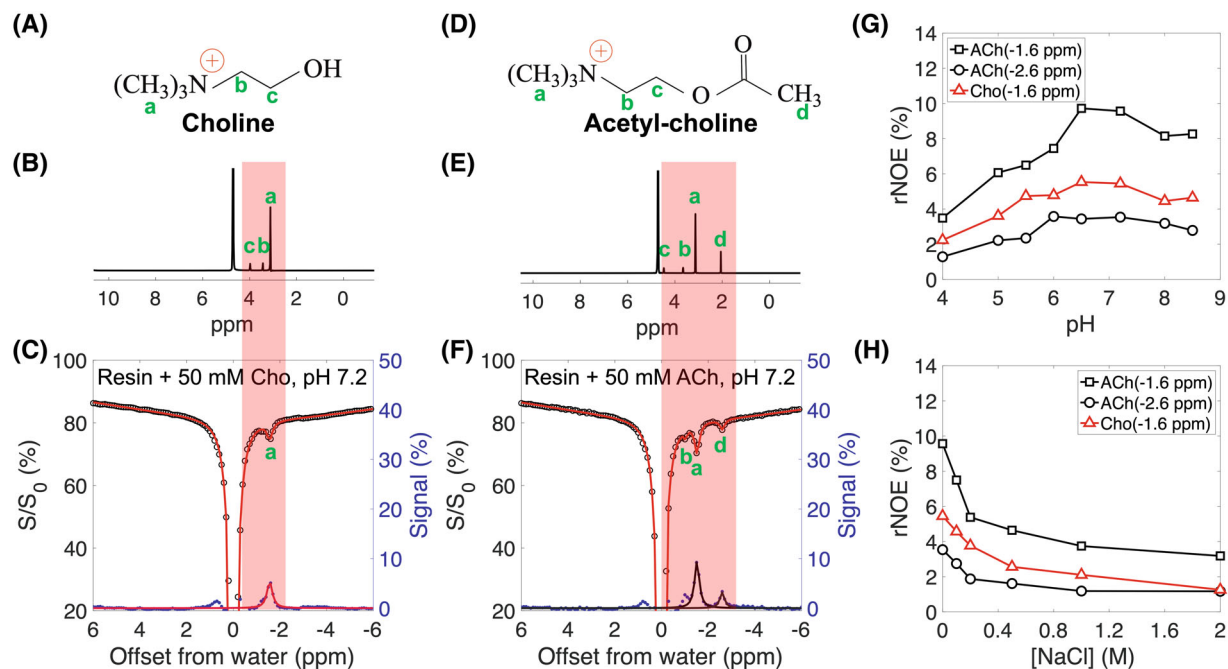
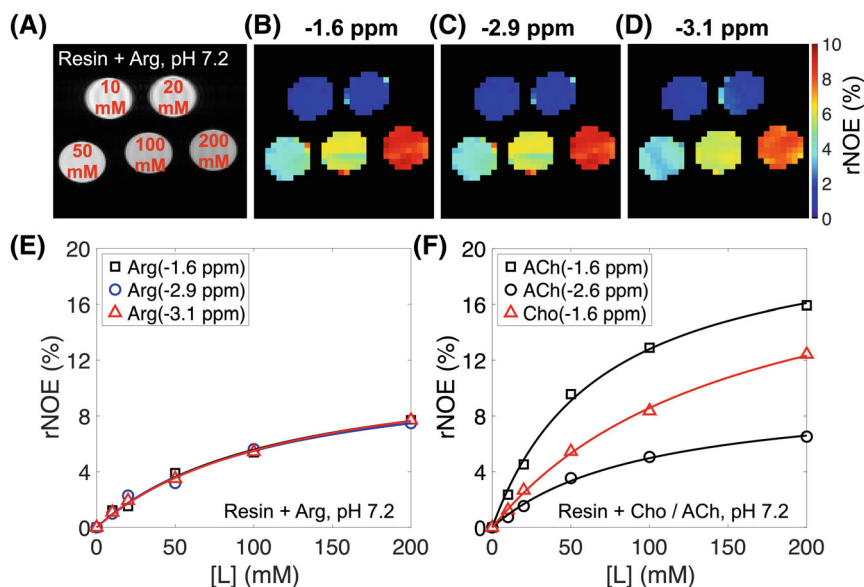


FIGURE 4 Z-spectroscopy of Cho and ACh solutions mixed with ionic resin. (A, D) Chemical structure of Cho and ACh, respectively. (B, E) ^1H NMR spectra of Cho and ACh solutions, respectively (50 mM, pH = 7.2, 5% $\text{H}_2\text{O}/95\%$ D_2O). Experimental (black circle) and fitted (red solid line) Z-spectra ($B_1 = 0.7 \mu\text{T}$, 4 s) of (C) Cho and (F) ACh solutions (50 mM, pH of 7.2) mixed with ionic resin (intensities on the left vertical axis). The Lorentzian fits of rNOE signals are shown at the bottom (scale on the right vertical axis). (G, H) The dependence of measured Cho and ACh rNOE signals on solvent pH and salt concentration, respectively

FIGURE 5 rNOE signal dependence on free ligand concentration. (A–D) Maps of Arg rNOE signals at -1.6 ppm (B), -2.9 ppm (C), and -3.1 ppm (D) at different concentrations (A). (E, F) The measured rNOE intensities (open markers) as a function of L-arginine, choline, acetyl-choline concentration in solvent, together with a fit (solid lines) using Equation (11)



or intra-molecular NOEs), and finally to water (via proton exchange or water exchange). Enhanced detection of bound ligands is achieved with an “MRI detectable” water signal. Using a three-step model, we show theoretically that the detected rNOE signal at the free ligand aliphatic proton frequency in the Z-spectra is a consequence of ligand binding to the immobile resin (Equation 11,

Figure 2), thus allowing evaluation of molecular binding affinities with ST MRI, using the “IMMOBILISE” concept.¹⁶

The analytical solution (Equation 11) and simulation data were in excellent agreement (Figure 2H) in describing the rNOE signal dependence. Theory (Figures 2A, C) and experimental data (Figures 5, S8) show that rNOE

TABLE 2 Estimated K_D , $rNOE_{max}$, and $\beta' \cdot \frac{[R_T]}{2[H_2O]}$ for L-arginine binding with ionic resin ($-COO^-$)

Ω_a^L (ppm)	K_D (mM)			$\frac{rNOE_{max}}{n_a}$ (%)			$\beta' \cdot \frac{[R_T]}{2[H_2O]}$ (%) ^b		
	-1.6	-2.9	-3.1	-1.6 ($n_a=2$) ^a	-2.9 ($n_a=2$)	-3.1 ($n_a=2$)	-1.6	-2.9	-3.1
0.3 μ T	101 \pm 47 ^c	150 \pm 51	122 \pm 55	3.0 \pm 0.7	3.6 \pm 0.7	3.1 \pm 0.7	8.1	7.2	8.1 ^d
0.5 μ T	147 \pm 37	147 \pm 40	139 \pm 40	6.0 \pm 0.8	6.0 \pm 0.9	5.6 \pm 0.9			
0.7 μ T	117 \pm 32	113 \pm 32	126 \pm 35	6.1 \pm 0.8	5.9 \pm 0.8	6.2 \pm 0.9			
Multi-B ₁ ^d	128 \pm 34	132 \pm 34	133 \pm 33	/	/	/	/	/	/

^a n_a is the number of protons in the aliphatic pool.

^b $\beta' \cdot \frac{[R_T]}{2[H_2O]}$ was obtained by fitting $rNOE_{max}$ as a function of B_1 (0.3, 0.5, and 0.7 μ T, Figure S9).

^cStandard deviations (SD) of K_D and $\frac{rNOE_{max}}{n_a}$ were obtained from 1000 Monte Carlo simulations of the ligand concentration curve (Equation 11) with 0.39% random noise, which was estimated from Z-spectra.

^dValues were obtained by the global fitting of experimental data at all three B_1 values simultaneously.

TABLE 3 Estimated K_D , $rNOE_{max}$, and $\beta' \cdot \frac{[R_T]}{2[H_2O]}$ for choline and acetyl-choline binding with ionic resin ($-COO^-$)

Ω_a^L (ppm)	K_D (mM)			$\frac{rNOE_{max}}{n_a}$ (%)			$\beta' \cdot \frac{[R_T]}{2[H_2O]}$ (%) ^a		
	Cho	ACh	ACh	Cho	ACh	ACh	Cho	ACh	ACh
0.3 μ T	145 \pm 56	91 \pm 18	105 \pm 62	2.0 \pm 0.3	2.1 \pm 0.2	2.4 \pm 0.6	3.9	2.5	4.4
0.5 μ T	194 \pm 73	61 \pm 10	109 \pm 58	2.9 \pm 0.6	2.3 \pm 0.2	3.4 \pm 0.9			
0.7 μ T	174 \pm 76	68 \pm 12	99 \pm 45	2.6 \pm 0.6	2.4 \pm 0.2	3.3 \pm 0.7	/	/	/
Multi-B ₁	160 \pm 22	70 \pm 8	103 \pm 30	/	/	/	/	/	/

For explanation of symbols, see Tables 1 and 2.

^a $\beta' \cdot \frac{[R_T]}{2[H_2O]}$ was obtained by fitting $rNOE_{max}$ at $B_1 = 0.3$ and 0.5 μ T (Figure S9).

signal intensities first depend linearly on the concentration of free ligand ($[L]$), but gradually plateau with increasing ligand concentration as the receptor occupancy saturates. A fast repetition of events and efficient magnetization transfer between relevant protons during ligand binding (cross relaxation), and proton/water exchange are prerequisite for sufficient signal enhancement (β' or $rNOE_{max}$). In other words, the binding rates (k_{off}), NOE cross-relaxation rates (σ) and exchange rates (k_{ew}) should be large enough to achieve a sufficient signal enhancement factor (β' , Equation 9). The maximum signal ($rNOE_{max}$) depends mainly on the rate-limiting step of the transfer. Several cases can be distinguished:

Case (1): k_{off} is rate-limiting ($k_{off} \ll \sigma_{ae}, k_{ew}$): then $\beta' \approx \frac{k_{off}}{\rho_w}$, and using $\alpha = 1$, we get:

$$rNOE_{max} \approx n_a \frac{k_{off}[R_T]}{2\rho_w[H_2O]} = n_a \frac{V_{max}}{2\rho_w[H_2O]} \quad (13)$$

V_{max} is the rate of the dissociation reaction when the complex is saturated. Similar to Michaelis-Menten enzyme

kinetics,²⁹ K_D is the concentration of substrate when the reaction reaches half of V_{max} . The ligand saturation curve can be used to determine V_{max} and K_D for resin-ligand binding.

Case (2): σ_{ae} is rate-limiting:

$$rNOE_{max} \approx n_a \frac{|\sigma_{ae}| [R_T]}{2\rho_w [H_2O]} \quad (14)$$

$rNOE_{max}$ becomes a measure of dipolar cross-relaxation effects, and is expected to be dependent on local geometry of binding but not pH. In this scenario, the $rNOE$ signal from ligand protons at different positions in the molecule would be different. However, the Arg data (Figures 3, 5) show that $rNOEs$ from different protons (c, d, e) are comparable, indicating that the spin-diffusion rate (σ_{ae}) is much faster than the binding and proton exchange rates.

Case (3): k_{ew} is rate-limiting:

$$rNOE_{max} \approx n_a \frac{k_{ew}}{\rho_w + k_{ew}} \cdot \frac{[R_T]}{2[H_2O]} \quad (15)$$

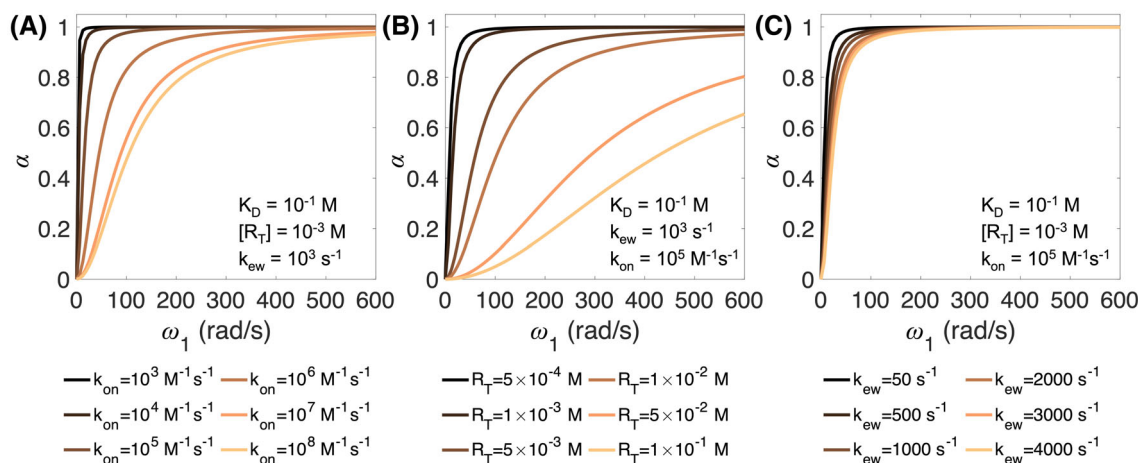


FIGURE 6 The dependence of the ligand proton pool saturation efficiency (α) on the radial frequency of B_1 is a function of (A) the binding rate (k_{on}), (B) the receptor concentration (R_T) and (C) proton exchange rates (k_{ew}). An increase in binding rate or solid pool size increases the saturation loss and more B_1 is needed to achieve saturation of the ligand protons

$rNOE_{max}$ becomes a measurement for the CEST effect of the receptor, and is expected to be pH sensitive (Figure S10).

The rNOEs also show a B_1 (or ω_1) dependence (Figures S9, 2G), which shows that the effective T_1 and T_2 in Equation (6) are shorter than those of free ligand. This indicates that the B_1 dependence results from a loss of saturation in the free ligand at a speed determined by k_{on} , the receptor concentration, and the speed of spin diffusion. When the ligand binds, all saturation is lost almost instantly due to spin diffusion (large σ). Using the Bloch simulations, we can gain some insight into this process (Figure 6). The simulations show that since σ is so large, we do not see any dependence on ω_1 when varying σ , but we do when varying k_{on} (Figure 6A) or the receptor concentration R_T (Figure 6B, thus the product k'_{on}). Interestingly, we even get a contribution of k_{ew} (Figure 6C), which is further transferring the saturation to water as an additional sink in this large spin bath. It is also worth noting that, in simulations, a larger B_1 generates larger rNOEs. However, in experiments, the B_1 amplitude needs to be optimized (Figure S7) to account for background signals (e.g., magnetization transfer contrast from immobile components, MTC, not included in the simulations) while maintaining sufficient saturation (α) of ligand protons (Figure 6); This MTC effect can be seen as a broad constant background of about 15% in Figures 3C, D and 4C, F for the saturation parameters used here.

The Arg Z-spectrum contains CEST signals from guanidinium and amide protons as well as rNOEs from aliphatic protons (Figures 3C, D). The CEST signal intensities depend on the free Arg concentration, while the rNOEs depend on the binding affinity as the Arg solution without resin does not show a NOE signal (Figure 3C). Salt

is known to reduce the retention of bound molecules,^{30,31} which is reflected in the data (Figure 3F). In contrast, CEST signals for Arg were found to decrease only slightly with salt content, confirming that the detected rNOEs are due to ionic binding.

Compared to Cho, ACh provides a simpler system to investigate the ST mechanism as it has no exchangeable protons and therefore no “intraligand rNOE” pathway (Figure 1C). Interestingly, ACh produces stronger rNOEs than Cho, indicating that transfer via “intermolecular rNOE” (Figures 1A, B) is sufficient to generate observable rNOE signals. Currently, we cannot distinguish experimentally the contributions of rNOEs via exchangeable protons (Figure 1A) and “bound water” (Figure 1B). However, the residence times of bound water on molecular surfaces are on the order of tens to hundreds of picoseconds (ps),^{32,33} while efficient proton NOE transfer would require coupling life times to be longer than nanoseconds.³² Therefore, the proton exchange relayed NOE pathway (Figure 1A) is expected to dominate for ACh.

The data in Figures 3 and 4 show that both CEST and rNOE signals are sensitive to pH. The exchange of Arg guanidinium protons (at +2 ppm) is base-catalyzed and its rate increases with pH.²⁸ The observed Arg CEST signal increased from pH 6 to 8, but then plateaued and decreased with pH as the spectra begin to enter the fast exchange regime (Figure 3E). The solvent pH also plays a critical role in determining the net charges (or protonation) of the ionic residues in both ligands and receptors (Figure S11), which modulates the electrostatic interactions and determines the binding equilibrium (K_D),²⁷ and thus observed rNOEs. For certain pH ranges, the pH dependence of rNOEs can therefore also be understood from the aspect of

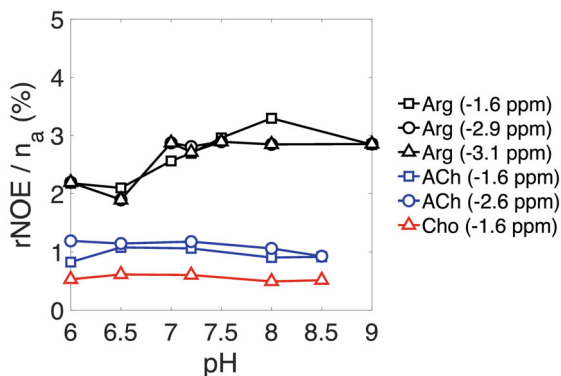


FIGURE 7 pH dependence of the rNOE signal normalized by n_a over the near to physiological pH range

ionic charges. The charge status of ionic groups can be estimated from their acid association constant (pK_A) and pH according to the Henderson-Hasselbalch approximation³⁴:

$$\log_{10} \frac{[A^-]}{[HA]} \approx \text{pH} - pK_A \quad (16)$$

where [HA] and $[A^-]$ are the molar concentrations of the weak acid and its conjugate base. The net charges of ACh and Cho (+1) are not significantly altered in the current pH range up to 8.5, due to a high pK_A (13.9). The observed lower rNOE signal from ACh and Cho below pH 6 (Figure 4G) may be due either to a gradual protonation of receptor groups ($-\text{COOH}$), and weaker binding (Figure S11) or the reduced exchange rates for exchangeable protons in the resin. Interestingly, at near physiological pH (pH 6 to 8, Figure 7), the rNOEs for ACh and Cho (as well as the molecular charges) are relatively constant, suggesting binding is not altered. In contrast, the rNOEs of Arg increases with pH (pH 6 to 8) and we therefore attribute the rNOE changes in Arg to be due to increased proton exchange rates for the guanidinium (position a, Figure 3A) and amide (position b) protons. The Arg rNOEs were found to decrease at strongly alkaline pH (above pH 8, Figure 3E), which may be caused by the Arg amino group becoming neutral and its binding becoming weaker (Figure S11). Therefore, the pH effects on rNOEs might be complicated: there are multiple possible saturation transfer pathways (both intermolecular rNOEs and intramolecular rNOEs, Figure 1). pH may affect binding initially and proton exchange in subsequent steps. It is clear from the equations that the pH effects on proton exchange will also affect overall rNOE efficiency,¹³ but this effect may not be the rate limiting over certain pH ranges, such as appears to be the case for Cho and ACh. Since the same resin is used for Arg, this means that the pH effect for the latter comes from the intra-ligand

exchangeable groups (guanidinium and amide protons), which also explains the pH sensitivity in the physiological range.

It can be seen from the simulation and experimental data that several factors (e.g., binding and transfer/exchange rates, ligand and receptor concentrations) affect the signal enhancement and thus the detection sensitivity of an experiment. Using 1% of water signal as a typical threshold for in vivo detection, our results for three small ligands demonstrate (Figure 5) the possibility of detection for concentrations as low as about 1 mM. This detection threshold is highly dependent on the types and quantity of available receptors, and we expect the imaging of μM levels of ligand to be possible if the receptor concentration (Figure 2E) or binding constant K_D (Figure 2F) can be optimized. From the simulations (Figure 2) and from the data (9 equivalent protons per ligand), we estimate that an rNOE of at least 1% (nominal in vivo detection threshold) is feasible if

- (I) the ligand concentration $> 100 \mu\text{M}$ (Figure 2I);
- (II) the total receptor (or binding site) concentration is at least $1 \mu\text{M}$ (Figure 2J) with an accompanying excess ligand concentration (1 mM);
- (III) the binding affinity K_D falls in the range of $10^{-1} \mu\text{M}$ to 10 M (Figure 2F);
- (IV) the ligand binding rate ($k'_{on} = k_{on}[R]$) is in the slow to intermediate regime in terms of the NMR time scale (10^1 to 10^6 s^{-1} , Figure 2F).

While the current study reports on in vitro experiments at an ultra-high field (17.6 T), performing the IMMOBILISE experiment at a clinically relevant field strength (3 T) still needs to be explored. To investigate this possibility, we simulated data comparing the signal at 17.6 T to 3 T (Figure S12). These data show the expected effect that rNOE signals at 3 T have similar linewidths in Hz, leading to broader lineshapes in ppm, proportionally to the ratio of the field strengths, with comparable amplitude. A characteristic of IMMOBILISE MRI is that the method is uniquely suited to imaging low-affinity (high nM to M range) binding of small molecules non-invasively. Some insight into possible in vivo targets and effect sizes can be obtained from previous spectroscopic studies that noticed a coupling between several metabolites (creatine, ethanol, lactate, glutamate/glutamine) and water mediated through semi-solid components.³⁵⁻⁴² These observable effects on millimolar signals indicate that these metabolites have binding affinities within the desired range. Based on this, it is reasonable to assume that in vivo Z-spectra already have contributions from IMMOBILISE pathways. In healthy tissue, these signals are difficult to

separate from other Z-spectral components but the IMMOBILISE signal may for instance become distinguishable in pathologies that cause an overexpression of receptors, such as many cancers. One could then foresee a change in endogenous metabolite signals but would more likely need to use exogenous ligands in the mM range to detect the IMMOBILISE effect. Although challenging due to signal sensitivity, when achieved, quantifying binding parameters in this situation may assist in evaluating disease progression or treatment effects.

5 | CONCLUSION

We demonstrated the MRI detection of ionic binding using saturation transfer (IMMOBILISE approach⁹), which provides a path to possible in vivo studies of molecular binding using MRI. To achieve a sensitivity of about 1% of water signal, a micromolar level concentration of receptor sites would be needed. The method in principle may be used to study not only ionic interactions, but also other types of reversible interactions, for instance, immobile receptor-substrate binding via van der Waals, hydrogen bonding, and hydrophobic effects.


ACKNOWLEDGMENTS

This research was supported by NIH grants EB015032, EB025295, and EB031771. Y.Z. receives support from National Natural Science Foundation of China (82171904), Key Laboratory for Magnetic Resonance and Multimodality Imaging of Guangdong Province (2020B1212060051) and SIAT Innovation Program for Excellent Young Researchers. C.B. thanks China Scholarship Council (201906970024) for financial support.

CONFLICT OF INTEREST

Drs. Yadav and van Zijl have a patent application for the IMMOBILISE method.


ORCID

Yang Zhou  <https://orcid.org/0000-0002-3920-3070>

Chongxue Bie  <https://orcid.org/0000-0002-1373-1983>

Jiadi Xu  <https://orcid.org/0000-0001-9698-5622>

Chao Zou  <https://orcid.org/0000-0002-6387-7809>

Nirbhay N. Yadav  <https://orcid.org/0000-0003-0802-9791>

REFERENCES

- Nakamura H. Roles of electrostatic interaction in proteins. *Q Rev Biophys.* 1996;29:1-90.
- Williamson MP. Chapter 3: applications of the NOE in molecular biology. In: Vol 65. Academic Press; 2009:77-109.
- Mayer M, Meyer B. Characterization of ligand binding by saturation transfer difference NMR spectroscopy. *Angew Chem Int Ed.* 1999;38:1784-1788.
- Lepre CA, Moore JM, Peng JW. Theory and applications of NMR-based screening in pharmaceutical research. *Chem Rev.* 2004;104:3641-3676.
- Fawzi NL, Ying J, Torchia DA, Clore GM. Probing exchange kinetics and atomic resolution dynamics in high-molecular-weight complexes using dark-state exchange saturation transfer NMR spectroscopy. *Nat Protoc.* 2012;7:1523-1533.
- van Zijl PCM, Yadav NN. Chemical exchange saturation transfer (CEST): what is in a name and what isn't? *Magn Reson Med.* 2011;65:927-948.
- Ward KM, Aletras AH, Balaban RS. A new class of contrast agents for MRI based on proton chemical exchange dependent saturation transfer (CEST). *J Magn Reson.* 2000;143:79-87.
- van Zijl PCM, Sehgal AA. Proton chemical exchange saturation transfer (CEST) MRS and MRI. *eMagRes.* 2016;5:1307-1332.
- van Zijl PCM, Lam WW, Xu J, Knutsson L, Stanisz GJ. Magnetization transfer contrast and chemical exchange saturation transfer MRI. Features and analysis of the field-dependent saturation spectrum. *NeuroImage.* 2018;168:222-241.
- van Zijl PC, Jones CK, Ren J, Malloy CR, Sherry AD. MRI detection of glycogen in vivo by using chemical exchange saturation transfer imaging (glycoCEST). *Proc Natl Acad Sci U S A.* 2007;104:4359-4364.
- Zhou Y, van Zijl PCM, Xu X, et al. Magnetic resonance imaging of glycogen using its magnetic coupling with water. *Proc Natl Acad Sci U S A.* 2020;117:3144-3149.
- Ling W, Regatte RR, Navon G, Jerschow A. Assessment of glycosaminoglycan concentration in vivo by chemical exchange-dependent saturation transfer (gagCEST). *Proc Natl Acad Sci U S A.* 2008;105:2266-2270.
- Zhou Y, van Zijl PCM, Xu J, Yadav NN. Mechanism and quantitative assessment of saturation transfer for water-based detection of the aliphatic protons in carbohydrate polymers. *Magn Reson Med.* 2021;85:1643-1654.
- Zeng H, Xu J, Yadav NN, et al. ¹⁵N heteronuclear chemical exchange saturation transfer MRI. *J Am Chem Soc.* 2016;138:11136-11139.
- Martinho RP, Novakovic M, Olsen GL, Frydman L. Heteronuclear 1D and 2D NMR resonances detected by chemical exchange saturation transfer to water. *Angew Chem Int Ed.* 2017;56:3521-3525.
- Yadav NN, Yang X, Li Y, Li W, Liu G, van Zijl PC. Detection of dynamic substrate binding using MRI. *Sci Rep.* 2017;7:10138.
- Bryant RG. The dynamics of water-protein interactions. *Annu Rev Biophys Biomol Struct.* 1996;25:29-53.
- Bloch F. Nuclear induction. *Phys Rev.* 1946;70:460.
- Gossert AD, Jahnke W. NMR in drug discovery: a practical guide to identification and validation of ligands interacting with biological macromolecules. *Prog Nucl Magn Reson Spectrosc.* 2016;97:82-125.
- Sanders CR. *Biomolecular Ligand-Receptor Binding Studies: Theory, Practice, and Analysis.* Vanderbilt University; 2010:1-43.
- Staahlberg J, Joensson B, Horvath C. Theory for electrostatic interaction chromatography of proteins. *Anal Chem.* 1991;63:1867-1874.

22. Kim M, Gillen J, Landman BA, Zhou J, Van Zijl PC. Water saturation shift referencing (WASSR) for chemical exchange saturation transfer (CEST) experiments. *Magn Reson Med*. 2009;61:1441-1450.
23. Chen L, Zeng H, Xu X, et al. Investigation of the contribution of total creatine to the CEST Z-spectrum of brain using a knockout mouse model. *NMR Biomed*. 2017;30:e3834.
24. Staby A, Jacobsen JH, Hansen RG, Bruus UK, Jensen IH. Comparison of chromatographic ion-exchange resins: V. Strong and weak cation-exchange resins. *J Chromatogr A*. 2006;1118:168-179.
25. Wishart DS, Knox C, Guo AC, et al. HMDB: a knowledgebase for the human metabolome. *Nucleic Acids Res*. 2009;37:D603-D610.
26. Klavan L, Crothers DM. High-resolution NMR of exchangeable protons in arginine, oligoarginines, and the arginine-rich histone tetramer. *Biopolymers*. 1979;18:1029-1044.
27. Jensen JH. Calculating pH and salt dependence of protein-protein binding. *Curr Pharm Biotechnol*. 2008;9:96-102.
28. Liepinsh E, Otting G. Proton exchange rates from amino acid side chains—implications for image contrast. *Magn Reson Med*. 1996;35:30-42.
29. Tzafiriri AR. Michaelis-Menten kinetics at high enzyme concentrations. *Bull Math Biol*. 2003;65:1111-1129.
30. Fekete S, Beck A, Veuthey J-L, Guillarme D. Ion-exchange chromatography for the characterization of biopharmaceuticals. *J Pharm Biomed Anal*. 2015;113:43-55.
31. Roosen-Runge F, Heck BS, Zhang F, Kohlbacher O, Schreiber F. Interplay of pH and binding of multivalent metal ions: charge inversion and reentrant condensation in protein solutions. *J Phys Chem B*. 2013;117:5777-5787.
32. Otting G, Liepinsh E, Wuthrich K. Protein hydration in aqueous solution. *Science*. 1991;254:974-980.
33. Bagchi B. Water dynamics in the hydration layer around proteins and micelles. *Chem Rev*. 2005;105:3197-3219.
34. Po HN, Senozan NM. The Henderson-Hasselbalch equation: its history and limitations. *J Chem Educ*. 2001;78:1499.
35. Helms G, Frahm J. Magnetization transfer attenuation of creatine resonances in localized proton MRS of human brain in vivo. *NMR Biomed*. 1999;12:490-494.
36. Meyerhoff DJ. Proton magnetization transfer of metabolites in human brain. *Magn Reson Med*. 1999;42:417-420.
37. Meyerhoff DJ, Rooney WD, Tokumitsu T, Weiner MW. Evidence of multiple ethanol pools in the brain: an in vivo proton magnetization transfer study. *Alcohol Clin Exp Res*. 1996;20:1283-1288.
38. Luo Y, Rydzewski J, de Graaf RA, Gruetter R, Garwood M, Schleich T. In vivo observation of lactate methyl proton magnetization transfer in rat C6 glioma. *Magn Reson Med*. 1999;41:676-685.
39. Meyerhoff D. Ethanol in human brain: relaxation and magnetization transfer. *Proc Int Soc Magn Reson Med*. 1998;1:193.
40. Kruiskamp M, De Graaf R, van Vliet G, Nicolay K. The ^1H -NMR signal of creatine/phosphocreatine from rat skeletal muscle shows a strong off-resonance magnetization transfer effect. *Magma*. 1997;5:27.
41. Kruiskamp MJ, van Vliet G, Nicolay K. Creatine kinase deficiency alters the off-resonance magnetization transfer effect of the creatine methyl ^1H -MR signal from mouse skeletal muscle. *Proc Int Soc Magn Reson Med*. 1998;1:384.
42. de Graaf RA, van Kranenburg A, Nicolay K. Off-resonance metabolite magnetization transfer measurements on rat brain in situ. *Magn Reson Med*. 1999;41:1136-1144.
43. Fayad LM, Salibi N, Wang X, et al. Quantification of muscle choline concentrations by proton MR spectroscopy at 3T: technical feasibility. *AJR Am J Roentgenol*. 2010;194:W73-W79.
44. Allard P, Helgstrand M, Härd T. A method for simulation of NOESY, ROESY, and off-resonance ROESY spectra. *J Magn Reson*. 1997;129:19-29.

SUPPORTING INFORMATION

Additional supporting information may be found in the online version of the article at the publisher's website.

Figure S1. Z-spectra for Arg solutions (100 mM, 20 °C, pH of 7.2, [NaCl] = 0) mixed with ionic resin as a function of B_1 . Lorentzian fitting was used to extract the signal.

Figure S2. Z-spectra for Arg solutions (100 mM, 20 °C, $B_1 = 0.7 \mu\text{T}$, [NaCl] = 0) mixed with ionic resin as a function of pH.

Figure S3. Z-spectra for Cho solutions (50 mM, 20 °C, pH of 7.2, [NaCl] = 0) mixed with ionic resin as a function of B_1 .

Figure S4. Z-spectra of Cho solution (50 mM, 20 °C, $B_1 = 0.7 \mu\text{T}$, [NaCl] = 0) mixed with ionic resin as a function of pH.

Figure S5. Z-spectra for ACh solutions (50 mM, 20 °C, pH of 7.2, [NaCl] = 0) mixed with ionic resin as a function of B_1 .

Figure S6. Z-spectra of ACh solution (50 mM, 20 °C, $B_1 = 0.7 \mu\text{T}$, [NaCl] = 0) mixed with ionic resin as a function of pH.

Figure S7. The peak intensities in Z-spectra as a function of B_1 power for 100 mM Arg (A), 50 mM Cho (B), and 50 mM ACh solution (B) mixed with ionic resin (pH of 7.2), respectively.

Figure S8. The rNOE signal dependence on free ligand concentration ([L]) for the aliphatic protons of interest in Arg (A-C), and Cho, and ACh (D-F) at B_1 values of 0.3 μT (A,D), 0.5 μT (B,E), 0.7 μT (C,F). 20 °C, pH = 7.2, [NaCl] = 0. Measured rNOE intensities in open markers, fitted values (using Equation 11) in solid lines.

Figure S9. The $rNOE_{max}$ dependence on B_1 fields. $\beta' \cdot \frac{[R]}{2[H_2O]}$ can be fitted from $rNOE_{max}$ (Equation 11).

Figure S10. The numerically simulated rNOE signal dependence on proton exchange rate (k_{ev}). $\omega_1 = 600 \text{ rad/s}$.

Figure S11. The molecular charges in ionic resin, Arg, Cho, and ACh at different pH. The ionic resin carboxylic acid group ($-\text{COOH}$, $\text{pKa} \sim 4.8$) is gradually deprotonated from acid pH to neutral pH, and then keeps stable with -1 net charge throughout the physiological pH range and at higher pH. The Arg carboxylic acid ($\text{pKa} \sim 2$) and guanidino ($(-\text{C}=[\text{NH}]-\text{NH}_2)$, $\text{pKa} \sim 13$) groups are always charged -1 and $+1$, respectively, in the pH 6–11 range. The Arg amino group ($-\text{NH}_3^+$, $\text{pKa} \sim 9$) has $+1$ charge when $\text{pH} < 8$, and de-protonates above that. The net charge of

Arg is changed from +1 to 0 for pH range 6–11. The Cho and ACh choline head groups ($pK_a \sim 13.9$) always have a +1 net charge.

Figure S12. Numerical simulations of rNOE signal in ST MRI of ligand binding at 3 T and 17.6 T. Simulation parameters (except the B_0 field) are in **Table 1** of main text, protocols are described above.

How to cite this article: Zhou Y, Bie C, van Zijl PCM, Xu J, Zou C, Yadav NN. Detection of electrostatic molecular binding using the water proton signal. *Magn Reson Med.* 2022;88:901-915. doi: 10.1002/mrm.29230